Monthly Notices of the ROYAL ASTRONOMICAL SOCIETY
MNRAS **447,** 846–857 (2015) doi:10.1093/mnras/stu2502

Stellar diameters and temperatures – VI. High angular resolution measurements of the transiting exoplanet host stars HD 189733 and HD 209458 and implications for models of cool dwarfs

Tabetha Boyajian,[1⋆] Kaspar von Braun,[2,3,4] Gregory A. Feiden,[5] Daniel Huber,[6,7] Sarbani Basu,[1] Pierre Demarque,[1] Debra A. Fischer,[1] Gail Schaefer,[8] Andrew W. Mann,[9†] Timothy R. White,[10] Vicente Maestro,[11] John Brewer,[1] C. Brooke Lamell,[1] Federico Spada,[12] Mercedes López-Morales,[13] Michael Ireland,[14] Chris Farrington,[8] Gerard T. van Belle,[4] Stephen R. Kane,[15] Jeremy Jones,[16] Theo A. ten Brummelaar,[8] David R. Ciardi,[17] Harold A. McAlister,[16] Stephen Ridgway,[18] P. J. Goldfinger,[8] Nils H. Turner[8] and Laszlo Sturmann[8]

Affiliations are listed at the end of the paper

Accepted 2014 November 21. Received 2014 November 21; in original form 2014 August 14

ABSTRACT

We present direct radii measurements of the well-known transiting exoplanet host stars HD 189733 and HD 209458 using the CHARA Array interferometer. We find the limb-darkened angular diameters to be $\theta_{\rm LD} = 0.3848 \pm 0.0055$ and 0.2254 ± 0.0072 mas for HD 189733 and HD 209458, respectively. HD 189733 and HD 209458 are currently the only two transiting exoplanet systems where detection of the respective planetary companion's orbital motion from high-resolution spectroscopy has revealed absolute masses for both star and planet. We use our new measurements together with the orbital information from radial velocity and photometric time series data, *Hipparcos* distances, and newly measured bolometric fluxes to determine the stellar effective temperatures ($T_{\rm eff} = 4875 \pm 43$, 6092 ± 103 K), stellar linear radii ($R_* = 0.805 \pm 0.016$, 1.203 ± 0.061 R$_\odot$), mean stellar densities ($\rho_* = 1.62 \pm 0.11$, 0.58 ± 0.14 $\rho_\odot$), planetary radii ($R_{\rm p} = 1.216 \pm 0.024$, 1.451 ± 0.074 $R_{\rm Jup}$), and mean planetary densities ($\rho_{\rm p} = 0.605 \pm 0.029$, 0.196 ± 0.033 $\rho_{\rm Jup}$) for HD 189733b and HD 209458b, respectively. The stellar parameters for HD 209458, an F9 dwarf, are consistent with indirect estimates derived from spectroscopic and evolutionary modelling. However, we find that models are unable to reproduce the observational results for the K2 dwarf, HD 189733. We show that, for stellar evolutionary models to match the observed stellar properties of HD 189733, adjustments lowering the solar-calibrated mixing-length parameter to $\alpha_{\rm MLT} = 1.34$ need to be employed.

Key words: techniques: interferometric – stars: fundamental parameters – stars: individual: HD 189733 – stars: individual: HD 209458 – stars: late-type – infrared: stars.

1 INTRODUCTION

Exoplanet characterization relies heavily on our ability to accurately describe the host star properties, as the properties of a planet are only known as well as those of its host star. A common approach is to use stellar atmosphere and evolutionary models to determine stellar properties from observables like spectral features and/or photometric colours. However, the comparison between these indirect calculations and direct measurements of both single and binary star radii and temperatures has consistently produced a discrepancy: directly determined values tend to be ∼5 per cent larger and ∼3 per cent cooler than their corresponding values predicted by models (e.g. Torres, Andersen & Giménez 2010; Boyajian et al. 2012). The source of this discrepancy is still unclear, but suggested explanations include stellar age, magnetic activity/starspots, close binary interactions, composition, convection, equation of state,

⋆E-mail: tabetha.boyajian@yale.edu
†Harlan J. Smith Fellow.

mixing-length theory, solar mixtures, or combinations of the above factors not being properly accounted for in the modelling processes.

Alleviating this dependence on models by directly measuring host star properties is a golden ticket to unbiased and *absolute* system properties. While empirical determination of the stellar radius is rare, select cases do exist where the host star radius is measured with long-baseline optical interferometry (LBOI) or asteroseismology. In the case of the former, LBOI has resolved the transiting exoplanet hosts GJ 436 (von Braun et al. 2012), 55 Cnc (Baines et al. 2008; van Belle & von Braun 2009; von Braun et al. 2011), and HD 189733 (Baines et al. 2007). Of these, only recent improvements to instruments and increased sensitivities and techniques have enabled measurements to determine these stellar radii to better than 5 per cent precision (3.1 per cent for GJ 436, von Braun et al. 2012; and 0.6 per cent for 55 Cnc, von Braun et al. 2011). For both transiting and non-transiting exoplanet hosts, the combination of the stellar angular size from LBOI, trigonometric parallax from *Hipparcos*, and bolometric flux via spectral energy distribution (SED) fitting allows for largely model-independent determination of stellar radii and effective temperatures (e.g. von Braun et al. 2014).

The latter technique of using asteroseismology to measure radii of transiting exoplanet host stars has been shown to be a fruitful resource in recent years compared to LBOI. The progress in this field is well described in Huber et al. (2013), who present results from the NASA *Kepler* mission of 77 exoplanet host stars in the *Kepler* field that have radii and masses via asteroseismology with uncertainties of $\sigma(R_*) \sim 3$ per cent and $\sigma(M_*) \sim 7$ per cent. Lastly, we note that the detections of circumbinary planets, i.e. transiting planets in eclipsing binary systems, have enabled the extraction of stellar/planetary radii to high precision through a full photometric-dynamical model (e.g. see Carter et al. 2011; Doyle et al. 2011). Unfortunately, although Welsh et al. (2012) predict that 1 per cent of close binary stars should have planets in such a perfect viewing configuration, few systems are known or well characterized.

This paper presents LBOI observations of two well-known transiting exoplanet host stars HD 189733 (Vmag = 7.70, K2 V; Gray et al. 2003) and HD 209458 (Vmag = 7.65, F9 V; Gray, Napier & Winkler 2001). We introduce our data in Section 2, and present the stellar and revised planetary properties in Section 3. In Section 4, we describe various model-dependent stellar properties in comparison with this work. In Section 5, we discuss scenarios to reconcile the discrepant results of the data with models for the lower mass host, HD 189733.

2 DATA

2.1 Interferometric observations

Interferometric observations were performed with the Center for High Resolution Astronomy (CHARA) Array, a long-baseline optical/infrared interferometer located at the historic Mount Wilson Observatory in California. The CHARA Array consists of six 1-m diameter telescopes in a Y-configuration where the distances between telescopes, referred to as the baseline B, range from ∼30 to 330 metres.

The predicted angular sizes of HD 189733 and HD 209458 are of the order of a few tenths of a milliarcsecond (e.g. see Boyajian, van Belle & von Braun 2014, and the discussion below). Thus, observations were conducted using the Precision Astronomical Visible Observations (PAVO) beam combiner with pairs of telescopes on the longest baseline configurations available in order to adequately resolve the stars. The PAVO beam combiner operates in the R band (Ireland et al. 2008), and routinely measures precise stellar angular diameters well under a milliarcsecond (Baines et al. 2012; Huber et al. 2012; Maestro et al. 2013; White et al. 2013).

Table 1. Log of interferometric observations.

Star UT date	Baseline	No. of obs	Calibrators
HD 189733			
2012/05/13	W1/E1	5	HD 189944, HD 190993
2012/05/14	W1/E1	1	HD 189944, HD 190993
HD 209458			
2012/08/23	S1/E1	6	HD 210516, HD 209380, HD 211733
2012/08/24	E1/W1	2	HD 210516, HD 209380, HD 211733
2012/10/04	S1/E1	4	HD 210516, HD 209380
2012/11/14	S2/E2	2	HD 210516, HD 209380

Note. For details on the interferometric observations, see Section 2.1.

A log of the observations is shown in Table 1. In summary, observations of each object were bracketed in time with several calibrator stars. Initial query of suitable calibrators is based on the JMMC Stellar Diameters Catalog (Bonneau et al. 2006, 2011).[1] We selected calibrators based upon their physical attributes: no known duplicity, low projected rotational velocity,[2] similar brightness compared to the science star at the wavelength of observation (within ∼1 mag), closer than 8 deg on the sky from science target, and, most importantly, to be unresolved point-like sources based on their estimated angular size (van Belle & van Belle 2005; Boyajian et al. 2013). Our calibrators, listed in Table 1, have estimated angular diameters ranging from $\theta_{\rm est} = 0.11$ to 0.19 mas (Bonneau et al. 2006, 2011). Our choice of using more than one calibrator with each science star allows the calibrators to be calibrated against one another. This is important especially when pushing the resolution limits to ensure no unwanted bias is present in the data.

Data for each star are reduced and calibrated using the standard reduction routines to extract calibrated squared-visibility measurements (V^2; for details, see Maestro et al. 2013; White et al. 2013). We fit the data to the functions for uniform disc and limb-darkened angular diameters defined in Hanbury Brown et al. (1974) using the solar metallicity (Table 3), R-band linear limb-darkening coefficients from Claret & Bloemen (2011). Limb darkening is dependent on both the stellar atmospheric properties of temperature and gravity, and we thus iterate on the coefficients to be consistent with the derived stellar properties (see Section 3, Table 3). Only one iteration was required for the values to converge. The final limb-darkening coefficients we use are $\mu_R = 0.67$ and 0.55 for HD 189733 and HD 209458, respectively. We assume a conservative 5 per cent uncertainty in these limb-darkening coefficients. Errors on the fitted angular diameter are computed from a Markov chain Monte Carlo (MCMC) simulation using 6400 realizations to account for uncertainties in the V^2 measurement, in the calibrator diameter (10 per cent), in limb-darkening coefficients (5 per cent), as well as the PAVO wavelength scale (5 per cent; detailed descriptions are found within Maestro et al. 2013; White et al. 2013). We obtain measured uniform disc diameters of $\theta_{\rm UD} = 0.3600 \pm 0.0046$ and 0.2147 ± 0.0066 mas and limb-darkened diameters of $\theta_{\rm LD} = 0.3848 \pm 0.0055$ and 0.2254 ± 0.0072

[1] http://www.jmmc.fr/catalogue_jsdc.htm

[2] Stars become oblate if rotating near critical velocities. The degree of oblateness depends on several factors, namely the stellar mass, (mean) radius, and the projected rotational velocity (Absil et al. 2008).

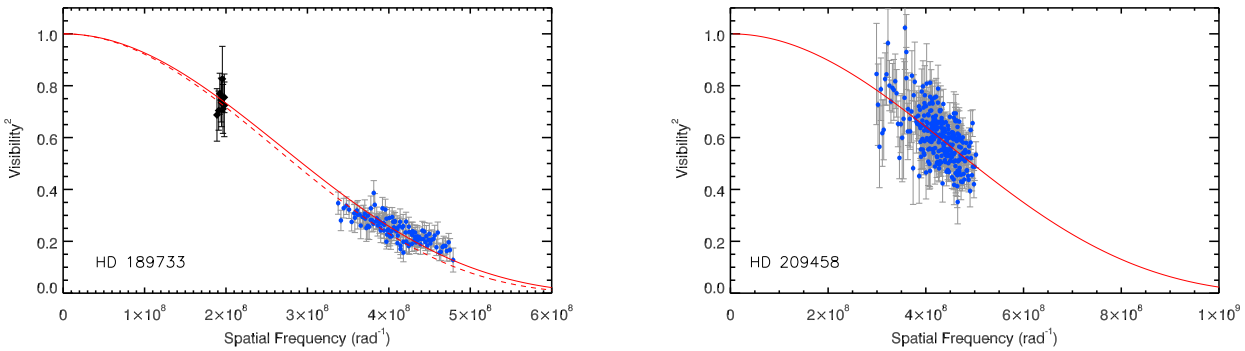

Figure 1. Plots of calibrated interferometric V^2 values and the limb-darkened V^2 values for HD 189733 (left) and HD 209458 (right). The blue dots represent the data presented in this work and the solid red line represents the *R*-band limb-darkened diameter fit for each star. The black diamonds represent the data from Baines et al. (2007), and the dashed red line represents their *H*-band limb-darkened diameter fit. Note that the V^2 functions are different for HD 189733 due to the limb-darkening coefficient, which is larger in the *R* band compared to the *H* band. The interferometric observations are described in Section 2.1.

mas for HD 189733 and HD 209458, respectively. Fig. 1 shows the data and the visibility curves for each star. These direct angular diameter measurements agree very well with both stars' predicted angular size using empirically calibrated surface-brightness relations from Boyajian et al. (2014): $\theta_{\rm SB} = 0.380 \pm 0.019$ for HD 189733 and $\theta_{\rm SB} = 0.228 \pm 0.011$ for HD 209458, consistent with our measured values to 0.005 and 0.003 mas (0.258σ and 0.002σ) for HD 189733 and HD 209458, respectively.

The CHARA Array was also used to measure the diameter of HD 189733 in Baines et al. (2007). This measurement was obtained using the CHARA Classic beam combiner in the *H* band ($\lambda = 1.67\,\mu$m) and yielded an angular diameter of $\theta_{\rm LD} = 0.377 \pm 0.024$ mas (6.7 per cent error). Our result presented here for HD 189733 agrees very well (0.008 mas; 0.46σ) with this result but reduces the measurement error by a factor of 3. The increased precision of our result is due to the choice of beam combiner that operates at shorter wavelengths (samples higher spatial frequencies), which increases the resolution by about a factor of 2.5 times for a given baseline. To illustrate this difference, we show the data from Baines et al. (2007) plotted with our own in Fig. 1.

Bakos et al. (2006) report the detection of an M-dwarf companion to HD 189733, with separation of ∼11 arcsec. Baines et al. (2007) discussed possible contamination of the interferometric measurements due to this companion, and rejected the possibility. We confirm that the interferometer's field of ∼2 arcsec (∼1 arcsec mask hole size plus seeing; Boyajian et al. 2008; Ireland et al. 2008) is too little in comparison to the binary separation and thus cannot bias the measurements presented here.

We caution that the angular size of HD 209458 is at the resolution limit of CHARA/PAVO, and that due to sensitivity limits, its calibrators are at most ∼30 per cent smaller than our target. Consequently, the measured diameter for HD 209458 (and subsequently derived stellar properties) may be affected by systematic errors in the estimated calibrator sizes.

2.2 Spectroscopic observations

Optical spectra of HD 189733 and HD 209458 were taken with the SuperNova Integral Field Spectrograph (SNIFS; Aldering et al. 2002; Lantz et al. 2004) on the University of Hawaii 2.2 m telescope atop Mauna Kea on 2014 September 4. SNIFS split the light into blue (0.32–0.52 μm) and red (0.51–0.97 μm) channels using a dichroic mirror. The spectral resolution was ≃800 and ≃1000 for the blue and red channels, respectively. Integration times were 33 and 50 s for HD 209458 and HD 189733, which yielded a median signal to noise ratio (SNR) of >300 per resolving element for both stars in the red channel but kept counts below the non-linear region of the detector.

Details of the SNIFS pipeline can be found in Bacon et al. (2001) and Aldering et al. (2006). Briefly, the pipeline performed dark, bias, and flat-field corrections and cleaned the data of bad pixels and cosmic rays, then calibrated the data based on arc lamp exposures taken at the same telescope pointing and time as the science data. The SNIFS pipeline applied an approximate flux calibration (based on archive data) and collapsed the three-dimensional data cubes into a one-dimensional spectrum using an analytic point spread function model. To achieve a more accurate flux calibration and correct telluric lines, we used spectra of the EG131, Fiege110, and BD+174708 spectrophotometric standards (Oke 1990) taken throughout the night and a model of the atmosphere above Mauna Kea (Buton et al. 2013). More details of our SNIFS reduction can be found in Gaidos et al. (2014).

Near-infrared spectra of HD 189733 and HD 209458 were taken with upgraded SpeX (uSpeX; Rayner et al. 2003) attached to the NASA Infrared Telescope Facility on Mauna Kea on 2014 August 26. Observations were performed in short cross-dispersed mode with the 1.6 arcsec × 15 arcsec slit. In this mode, uSpeX provided continuous coverage from 0.7 to 2.5 μm at a resolution of ≃400. Each target was placed at two positions along the slit (A and B) and observed in an ABBA pattern to accurately subtract the sky background by differencing. At least eight spectra were taken this way, which gave a median SNR > 200 for each star. To remove effects from large telescope slews, we obtained flat-field and argon lamp calibration sequences after each target. To correct for telluric lines, we observed an A0V-type star immediate after each target and within 0.1 airmasses.

Spectra were extracted using version 4.0 of the SPEXTOOL package (Cushing, Vacca & Rayner 2004), which performed flat-field correction, wavelength calibration, sky subtraction, and extraction of the one-dimensional spectrum. Multiple exposures were combined using the IDL routine XCOMBXPEC. A telluric correction spectrum was constructed from each A0V star and applied to the relevant spectrum using the XTELLCOR package (Vacca, Cushing & Rayner 2003). The uSpeX orders were merged using the XMERGEORDERS tool.

Optical and NIR spectra were joined for each star using the overlapping region (0.7–0.9 μm), first by scaling the optical to match the NIR data, then by replacing the overlapping region with the weighted mean of the two spectra at each wavelength element.

Table 2. Photometry used in SED fitting.

Star	Photometric system	Filter	Value	Uncertainty	Reference
HD 189733	Stromgren	*u*	10.413	0.08	Olsen (1993)
HD 189733	Stromgren	*v*	9.172	0.08	Olsen (1993)
HD 189733	Stromgren	*b*	8.203	0.08	Olsen (1993)
HD 189733	Stromgren	*y*	7.676	0.08	Olsen (1993)
HD 189733	Stromgren	*u*	10.4	0.05	Kotoneva et al. (2002)
HD 189733	Stromgren	*b*	8.192	0.05	Kotoneva et al. (2002)
HD 189733	Stromgren	*v*	9.161	0.05	Kotoneva et al. (2002)
HD 189733	Stromgren	*y*	7.665	0.05	Kotoneva et al. (2002)
HD 189733	Stromgren	*y*	7.67	0.05	Kotoneva et al. (2002)
HD 189733	2MASS	*J*	6.073	0.027	Cutri et al. (2003)
HD 189733	2MASS	*H*	5.587	0.027	Cutri et al. (2003)
HD 189733	2MASS	*Ks*	5.541	0.015	Cutri et al. (2003)
HD 189733	Johnson	*U*	9.241	0.1	Koen et al. (2010)
HD 189733	Johnson	*B*	8.578	0.03	Koen et al. (2010)
HD 189733	Johnson	*V*	7.648	0.03	Koen et al. (2010)
HD 189733	Cousins	*Rc*	7.126	0.03	Koen et al. (2010)
HD 189733	Cousins	*Ic*	6.680	0.03	Koen et al. (2010)
HD 189733	Johnson	*V*	7.680	0.05	Bailer-Jones (2011)
HD 209458	Stromgren	*u*	9.462	0.08	Olsen (1983)
HD 209458	Stromgren	*v*	8.558	0.08	Olsen (1983)
HD 209458	Stromgren	*b*	8.020	0.08	Olsen (1983)
HD 209458	Stromgren	*y*	7.650	0.08	Olsen (1983)
HD 209458	Stromgren	*u*	9.46	0.05	Olsen (1994)
HD 209458	Stromgren	*u*	9.439	0.05	Olsen (1994)
HD 209458	Stromgren	*b*	8.018	0.05	Olsen (1994)
HD 209458	Stromgren	*b*	8.015	0.05	Olsen (1994)
HD 209458	Stromgren	*v*	8.556	0.05	Olsen (1994)
HD 209458	Stromgren	*v*	8.548	0.05	Olsen (1994)
HD 209458	Stromgren	*y*	7.648	0.05	Olsen (1994)
HD 209458	Stromgren	*y*	7.663	0.05	Olsen (1994)
HD 209458	Stromgren	*u*	9.443	0.08	Hauck & Mermilliod (1998)
HD 209458	Stromgren	*v*	8.546	0.08	Hauck & Mermilliod (1998)
HD 209458	Stromgren	*b*	8.011	0.08	Hauck & Mermilliod (1998)
HD 209458	Stromgren	*y*	7.650	0.08	Hauck & Mermilliod (1998)
HD 209458	Johnson	*V*	7.65	0.01	Høg et al. (2000)
HD 209458	Johnson	*B*	8.18	0.02	Høg et al. (2000)
HD 209458	Johnson	*V*	7.639	0.02	Kharchenko (2001)
HD 209458	Johnson	*B*	8.230	0.04	Kharchenko (2001)
HD 209458	2MASS	*J*	6.591	0.011	Cutri et al. (2003)
HD 209458	2MASS	*H*	6.366	0.035	Cutri et al. (2003)
HD 209458	2MASS	*Ks*	6.308	0.021	Cutri et al. (2003)
HD 209458	Johnson	*V*	7.693	0.063	Droege et al. (2006)
HD 209458	Johnson	*V*	7.640	0.014	Kharchenko et al. (2007)

Note. Photometry data used for SED fitting. See Section 2.3 for details.

The final spectra reflect the SEDs for each star with continuous wavelength coverage from 0.32 to 2.5 μm. Based on repeated observations taken in the same way and comparisons of spectra from other instruments suggests the relative flux calibration of these spectra are good to better than 1 per cent (Mann, Gaidos & Ansdell 2013).

2.3 Bolometric fluxes

We calculated bolometric flux ($F_{\rm bol}$) following the procedure from Mann et al. (2013). To summarize, we obtained flux-calibrated literature photometry for each star, which are listed in Table 2. We then computed corresponding synthetic magnitudes from the spectra of each star (Section 2.2). Each spectrum was scaled to minimize the difference (in standard deviation) between synthetic and literature photometry.

While zero-points for most of the photometry are generally only calibrated to 1–2 per cent (Bohlin, Gordon & Tremblay 2014), we use updated zero-points and filter profiles from Bessell & Murphy (2012) and Mann & von Braun (2014), which are calibrated to STIS spectra and generally accurate to 1 per cent. HD 189733 is known to be variable by 0.03 mag in *V*, although less so at red wavelengths. Both issues are factored in our estimate of the error in $F_{\rm bol}$. Interstellar extinction is set to zero for both targets, due to the small distances to the stars and the unusually tenuous interstellar medium around the solar neighbourhood out to a radius of 70 pc (Aumer & Binney 2009). This is consistent with the $E(B-V) = 0$ for both stars (Ramírez & Meléndez 2005; Árnadóttir, Feltzing & Lundström 2010).

We find $F_{\rm bol} = 2.785 \pm 0.015$ and 2.331 ± 0.020 (10^{-8} erg s^{-1} cm^{-2}) for HD 189733 and HD 209458, respectively. These bolometric fluxes agree within a per cent with values derived

Table 3. Stellar and planetary properties.

Property	HD 189733 Value	HD 189733 Reference	HD 209458 Value	HD 209458 Reference
$\theta_{\rm LD}$ (mas)	0.3848 ± 0.0055	This work (Section 2.1)	0.2254 ± 0.0072	This work (Section 2.1)
$F_{\rm Bol}$ (10^{-8} erg s^{-1} cm^{-2})	2.785 ± 0.058	This work (Section 2.3)	2.331 ± 0.051	This work (Section 2.3)
L_* ($L_\odot$)	0.328 ± 0.011	This work (Section 3.1)	1.788 ± 0.147	This work (Section 3.1)
R_* ($R_\odot$)	0.805 ± 0.016	This work (Section 3.1)	1.203 ± 0.061	This work (Section 3.1)
$T_{\rm eff}$ (K)	4875 ± 43	This work (Section 3.1)	6092 ± 103	This work (Section 3.1)
[Fe/H] (dex)	-0.03 ± 0.08	Torres, Winn & Holman (2008)	0.00 ± 0.05	Torres et al. (2008)
$R_{\rm p}/R_*$	$0.155\,313 \pm 0.000\,188$	Agol et al. (2010)	$0.124\,03 \pm 0.000\,43$	Beaulieu et al. (2010)
$R_{\rm p}$ ($R_{\rm Jup}$)	1.216 ± 0.024	This work (Section 3.2)	1.451 ± 0.074	This work (Section 3.2)
M_* ($M_\odot$)	0.846 ± 0.049	de Kok et al. (2013)	1.00 ± 0.22	Snellen et al. (2010)
$M_{\rm p}$ ($M_{\rm Jup}$)	1.162 ± 0.058	de Kok et al. (2013)	0.64 ± 0.09	Snellen et al. (2010)
$\log g_{\rm p}$	3.29 ± 0.02	This work (Section 3.2)	2.88 ± 0.07	This work (Section 3.2)
$\log g_*$	4.56 ± 0.03	This work (Section 3.2)	4.28 ± 0.10	This work (Section 3.2)
$\rho_{\rm p}$ ($\rho_{\rm Jup}$)	0.605 ± 0.029	This work (Section 3.2)	0.196 ± 0.033	This work (Section 3.2)
ρ_* ($\rho_\odot$)	1.62 ± 0.11	This work (Section 3.2)	0.58 ± 0.14	This work (Section 3.2)

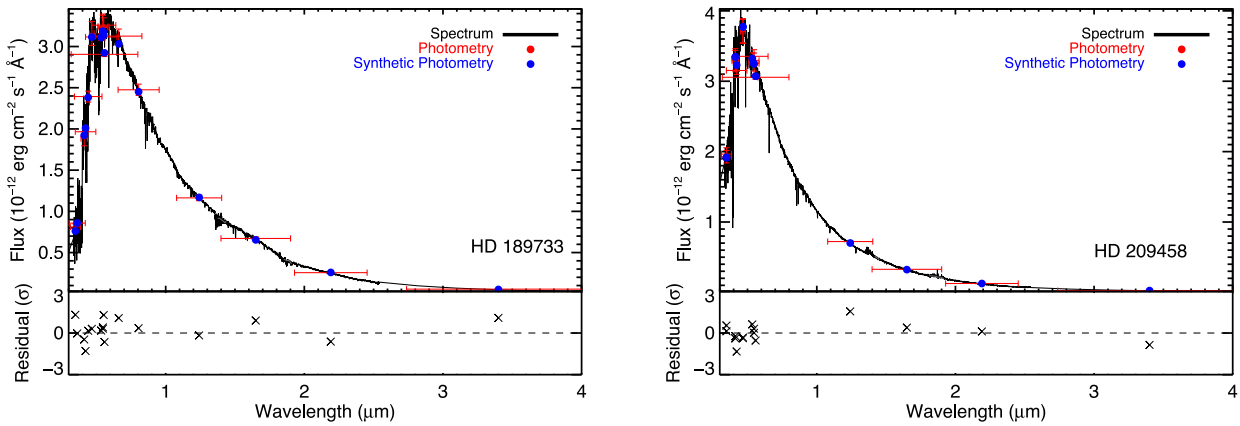

Figure 2. SEDs for HD 189733 (left) and HD 209458 (right). The (black) spectra represent the joined SNIFS+uSpeX spectra. The (red) points indicate photometry values from the literature. 'Error bars' in x-direction represent bandwidths of the filters used. The (blue) points show the flux value of the spectral template integrated over the filter transmission. The lower panel shows the residuals around the fit in units of standard deviations. For details, see Section 2.3, and for results, see Table 3.

in Casagrande et al. (2011) via the infrared flux method (2.7666 and 2.3379, same units). Finally, in order to account for unknown systematic effects due to, for example, uncertainties in photometric magnitude zero-point calculations, correlated errors in the photometry, potential errors in the spectral templates, filter transmission functions, etc., we add a 2 per cent uncertainty to each $F_{\rm bol}$ uncertainty value in quadrature (e.g. see discussion in Bohlin et al. 2014, in particular their sections 3.2.1– 3.2.3). Final results are in Table 3, and we show our calibrated spectra in Fig. 2.

3 STELLAR AND PLANETARY PROPERTIES

3.1 General stellar properties

Hipparcos parallaxes from van Leeuwen (2007) are used in combination with our measured angular sizes (Section 2.1) to determine linear radii for each star. Furthermore, we are able to calculate the absolute bolometric luminosity for each star with *Hipparcos* parallaxes and bolometric fluxes from Section 2.3. Lastly, by rearranging the Stefan–Boltzmann equation in terms of observable quantities, we derive effective temperatures for both stars:

$$T_{\rm eff} = 2341(F_{\rm bol}/\theta_{\rm LD}^2)^{0.25}, \quad (1)$$

where the constant 2341 is used for convenient units: the bolometric flux $F_{\rm bol}$ in 10^{-8} erg s^{-1} cm^{-2}, the limb-darkened angular diameter $\theta_{\rm LD}$ in milliarcsecond, and the effective temperature $T_{\rm eff}$ in kelvin. For both HD 189733 and HD 209458, we present these radii, luminosities, and effective temperatures in Table 3. The errors on each variable are propagated in quadrature for the final parameter error value listed.

3.2 The unique circumstances and available auxiliary data for HD 189733 and HD 209458

Both HD 189733 and HD 209458 are known hosts to transiting exoplanets (Charbonneau et al. 2000; Henry et al. 2000; Bouchy et al. 2005). The analysis of a transiting exoplanet's photometric light curve directly measures the planet-to-star radius ratio $R_{\rm p}/R_*$ (Winn 2010; Seager 2011). A transit signature in a photometric light curve is typically confirmed to be planetary in nature with follow-up radial velocity observations. Such follow-up observations detect radial velocity shifts of the host star from the planet's gravitational pull as it orbits. This measurement provides the system's mass function, or sum of the masses, when the inclination is known, but not individual masses of both components. New detection techniques

have recently allowed for the detection of spectral lines originating from the planet itself (see de Kok et al. 2014 for details and review of the field). These measurements of the planet's orbital velocity K_2 yields the system mass ratio, $K_2/K_1 = M_1/M_2$, where $K_{1,2}$ are the radial velocity semi-amplitudes and $M_{1,2}$ are the masses of each component. Thus applying this method to observed transiting planetary systems where the orbital inclination is known from the light-curve solution provides *absolute* masses of both the host star and the transiting planet, just like an eclipsing binary system. Currently, our targets are the only two transiting exoplanet systems have been observed in this way. The pioneering work by Snellen et al. (2010) was the first to observe this in HD 209458. de Kok et al. (2013) later announced the successful detection of the planet's radial velocities to the HD 189733 system, which was confirmed with independent efforts in Rodler, Kürster & Barnes (2013).

In this work, we take advantage of the wealth of knowledge for both the HD 189733 and HD 209458 systems, as described in the above text. For the remainder of this paper, we assume the R_p/R_* measured from 8 μm *Spitzer* observations, where the data are least influenced by limb darkening (references used are Agol et al. 2010 for HD 189733 and Beaulieu et al. 2010 for HD 209458). We further use the measured stellar and planetary masses from de Kok et al. (2013) for HD 189733 and Snellen et al. (2010) for HD 209458. All values and references mentioned are also shown in Table 3.

Using the planet-to-star radius ratio in combination with our measured stellar radius, we are able to *empirically* determine the planetary radii of $1.216 \pm 0.024 R_{\rm Jup}$(2.2 per cent) and $1.451 \pm 0.074 R_{\rm Jup}$(5.4 per cent) for HD 189733 and HD 209458, respectively. Furthermore, knowing both the stellar and planetary mass and radius, it is then straightforward to calculate the surface gravity $\log g$ ($\log g \propto M/R^2$) and mean density ρ ($\rho \propto M/R^3$) of each component in the system. These values are listed in Table 3. The density of HD 189733b ($\rho_p = 0.802 \pm 0.038$ g cm^{-3}) and HD 209458b ($\rho_p = 0.260 \pm 0.043$ g cm^{-3}) are much like that of butter and cork, respectively.[3]

4 PREVIOUSLY DETERMINED HOST STAR PROPERTIES

The first direct measurement of HD 189733's radius was made by Baines et al. (2007, Section 2.1). We have shown that our data, taken at much higher resolution, agree with this result by well under 1σ, as well as improve the error by a factor of 4.5. No prior direct measurements of the radius of HD 209458 are published for comparison.

Over the years, estimates of the stellar properties of each star have been made using many techniques. We compare our values to the transiting exoplanet host star properties from Torres et al. (2008) and Southworth (2010, 2011).[4] The Torres et al. (2008) and Southworth (2010) papers both consist of a rigorous, uniform analysis using all available literature data on known transiting systems at the time. Similarly, their efforts make use of the photometric (a/R_*) measured from the light curve (Seager & Mallén-Ornelas 2003) as an external constraint on surface gravity, expanding upon the method developed by Sozzetti et al. (2007). Torres et al. (2008) derive stellar properties (mass, radius, luminosity, surface gravity, and age) by fitting Yonsei–Yale (Y^2) evolutionary models (Yi et al. 2001; Yi, Kim & Demarque 2003; Demarque et al. 2004) to the spectroscopically determined $T_{\rm eff}$ and [Fe/H], using the photometric (a/R_*) as evolutionary indicator. Host star properties derived in Southworth (2010, 2011) are derived by a similar approach, using up to six different evolutionary models as well as empirically established relations derived from well-studied eclipsing binaries. Other select references to determine stellar properties are also touched upon in the discussion to follow, though the vast amount of literature references for each star makes a complete comparison demanding, with very little return.

The mean stellar density computed by our method (Table 3) and the density determined via the photometric time series analysis are the most fundamentally derived values to compare, since they are largely independent of models. The stellar density derived for HD 189733 and HD 209458 agree well with our measurements within $\sim 1.5\sigma$ for HD 189733 and within 1.0σ for HD 209458 (Torres et al. 2008; Southworth 2010).

Stellar radii are determined indirectly, generally via stellar evolutionary models, using the results from high-resolution spectroscopic observations with stellar atmosphere models as inputs (see above). In this way, Torres et al. (2008) find the radius for HD 209458 to be 1.155 ± 0.015 R$_\odot$, agreeing well with our value within 0.8σ (0.05 R$_\odot$). The detailed, yet indirect estimate of HD 209458's stellar radius by Cody & Sasselov (2002) of $R = 1.18 \pm 0.1$ R$_\odot$ agrees with our value within 0.2σ (0.02 R$_\odot$). Note that since HD 209458 is located at a distance of nearly 50 pc, the errors in the *Hipparcos* parallax contribute significantly to our linear radius calculation. For this work, we assume the parallax from the van Leeuwen (2007) reduction ($\pi = 20.15 \pm 0.80$ mas, distance =49.63 ± 1.97 pc). However, if we were to use the Perryman et al. (1997) parallax value from the first *Hipparcos* reduction ($\pi = 21.24 \pm 1.00$ mas, distance =47.08 ± 2.22 pc), our radius measurement would be $R_* = 1.14 \pm 0.06$ R$_\odot$. While this radius value is still consistent within errors of the adopted values mentioned above, it underlines the importance of having an accurate distance measurement to HD 209458 in order to constrain our results better.

On the other hand, the radius for HD 189733 from Torres et al. (2008), $R_* = 0.756 \pm 0.018$ R$_\odot$, is 2σ (0.05 R$_\odot$) smaller than our measurement. The significant offset of the Torres et al. (2008) radius and our measurement for HD 189733 is likely a result from the evolutionary model not being able to reliably reproduce observed stellar parameters in later type stars (e.g. Boyajian et al. 2012). This detail was addressed in Torres et al. (2008) for the M-dwarf transiting planet host GJ 436, and thus the stellar properties for that star came from a specialized method described in Torres (2007). This semi-empirically determined radius value of GJ 436 was confirmed by von Braun et al. (2012), who directly measured its radius using LBOI. The two values agree by $\sim 0.4\sigma$ (2 per cent). The evolutionary model predictions however yield a radius >10 per cent smaller for this star, a known shortcoming in the models for low-mass stars, as discussed in Torres et al. (2008) and von Braun et al. (2012).

While this deficiency in stellar models is generally viewed as a concern for the stellar properties of M-dwarfs, similar incompatibilities exist for more massive stars. As shown in Boyajian et al. (2012), the observed radii and temperatures of single, K- and M-dwarfs were discrepant with the predictions from the Dartmouth models (DSEP; Dotter et al. 2008). Specifically, Boyajian et al. (2012) found that models overestimate temperatures by ∼3 per cent, and underestimate radii by ∼5 per cent for stars cooler than about 5000 K. This

[3] http://www.iem-inc.com/information/tools/densities – 'I can't believe it's not butter', *Fabio*.

[4] The planetary density in Southworth (2010) is corrected in Southworth (2011) using the right scaling constant for Jupiter's density, effectively lowering previous densities by ∼7 per cent. Southworth (2009) provides a lot of the background framework to the sequentially later papers cited here.

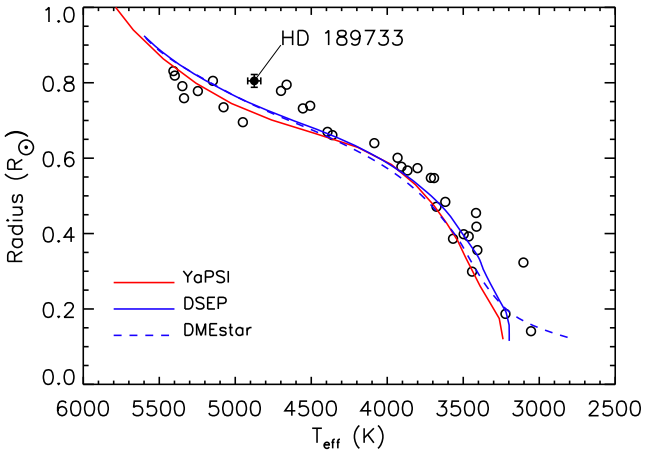

Figure 3. Radius–temperature plot showing the position of HD 189733 (filled point) with the low-mass stars in Boyajian et al. (2012, open points). Also plotted are solar abundance, 5 Gyr isochrones from the DSEP (solid blue line), DMEstar (dashed blue line), and YaPSI (solid red line) model grids. Refer to Section 4 for details.

discrepancy was independently confirmed by Spada et al. (2013) using YaPSI (Yale-Potsdam Stellar Isochrones), the most recent set of tracks and isochrones calculated with the Yale Rotational stellar Evolution Code (YREC). In Fig. 3, we show the measured radius and effective temperature of HD 189733 (solid point) with the low-mass stars that have directly measured radii and temperatures in Boyajian et al. (2012, open points).

Also displayed in Fig. 3 are solar metallicity, 5 Gyr isochrones from the Dartmouth Stellar Evolution Database (DSEP; Dotter et al. 2008), DMEstar (Dartmouth Magnetic Evolutionary Stellar Tracks And Relations; updated DSEP grid of models, described briefly in Muirhead et al. 2014 and Malo et al. 2014), as well as YaPSI (Spada et al. 2013). Fig. 3 shows that most of the points with $T_{\rm eff} < 5000$ K fall above the model isochrone predictions. The position of HD 189733 in this plot is consistent with the parameter space where model predictions deviate from the directly measured astrophysical properties for the lower mass stars (Boyajian et al. 2012; Spada et al. 2013).

5 HARMONIZING STELLAR EVOLUTIONARY MODEL PREDICTIONS WITH OBSERVATIONAL DATA

In Section 4, we show that the properties of HD 209458 are consistent with model predictions; however, HD 189733 shows potential for significant disagreement. As an initial comparison to models, the properties of HD 189733 are interpolated on to a 5 Gyr, solar metallicity isochrone from the Dartmouth series (Dotter et al. 2008). When using stellar luminosity as the dependent variable, the model predicted mass is 0.805 $M_\odot$, consistent with observations. However, the model $T_{\rm eff} = 5028$ K and $R = 0.756$ $R_\odot$ are 150 K (3.6σ) too hot and 0.05 $R_\odot$ (2.9σ) too small, respectively. If the empirical mass is used as the dependent variable instead, models predict $R = 0.796$ $R_\odot$, $T_{\rm eff} = 5225$ K and $L = 0.4245$ $L_\odot$. In this scenario, the radius is consistent with observations, but the $T_{\rm eff}$ and luminosity are too high by 350 K (8σ) and 0.1 $L_\odot$ (9σ), respectively. Model predictions are therefore not compatible with the empirical data.

Here, we explore various explanations for the discrepancies between the model predictions and the empirical data. We investigate the effects of age, composition, and how convection is treated in models given the constraints provided by the observational data. Given the observational results (Table 3), we are able to deduce the likely cause of the model offsets for the predicted properties of HD 189733 is due to the treatment convection and the choice of the mixing-length parameter $\alpha_{\rm MLT}$ (see Section 5.3.1).

5.1 Age

Models with masses in the 0.8 $M_\odot$ range undergo non-negligible evolution along the main sequence (MS). Thus, adoption of a 5 Gyr isochrone is not exactly appropriate. Allowing for variations in age is equivalent to investigating whether models of different masses provide a more consistent fit to the data. However, we find that no models simultaneously fit the $T_{\rm eff}$ and radius of HD 189733 at an age younger than that of the Universe. In all cases, when a given model mass track fits the measured radius, the $T_{\rm eff}$ is too hot. Conversely, when the models match the measured $T_{\rm eff}$, the radius is too small. However, this is only considering ages along the MS.

Along the pre-main-sequence (pre-MS), at an age near 40 Myr, models with masses around 0.82 $M_\odot$ match the complete set of observed properties. Around 40 Myr, models suggest a star of this mass is nearing the MS, having developed a small convective core prior to the *p*–*p* chain coming into full equilibrium, which brings about the establishment of a radiative core. Although these pre-MS models are in agreement with the observed stellar properties, other factors indicate that HD 189733 is unlikely to be a pre-MS star. Evidence comes from its derived rotation period (∼11 d), its low levels of magnetic activity (Pillitteri et al. 2010; Guinan 2013), and lack of any detectable lithium in the spectrum (Mishenina et al. 2012), all of which indicate HD 189733 is an MS star.

5.2 Composition

Departures from a strictly-scaled solar composition could, in principle, provide better agreement between observations and the stellar models. These departures include differences in the bulk metallicity, variations in α-element abundances, a non-solar helium abundance, and also the solar heavy element mixture.

5.2.1 Metallicity

To fit the observed $T_{\rm eff}$ and radius, models require a scaled solar metallicity of [M/H] = +0.2 dex and predict an age of approximately 10 Gyr. Abundance analyses however find [M/H] = -0.03 ± 0.08 dex, with a tendency for mildly subsolar metallicity (Bouchy et al. 2005; Torres et al. 2008). Individual element abundances show variation consistent with [M/H] within the uncertainties. One prominent exception is oxygen, which appears underabundant in HD 189733 by roughly 0.2 dex ([O/Fe] = −0.2 dex; Mishenina et al. 2013) compared to the Sun. Thus, there does not appear to be evidence for a supersolar metallicity in HD 189733's atmosphere which is required by the models to fit the observations.

5.2.2 α-element enhancement

In the light of the measured underabundance of oxygen, it is possible that the star has a non-solar-like abundance of α-elements. We test this idea with models having [α/Fe] = −0.2 and +0.2 dex as a proxy for variations in oxygen abundance. Increasing [α/Fe] has the effect of reducing both the $T_{\rm eff}$ and radius of the model whereas decrease [α/Fe] has the opposite effect. Agreement is found using

[α/Fe] = +0.2 dex at an age of roughly 9 Gyr, but this is in disagreement with the observed oxygen abundance of HD 189733 (see above). Models incorporating individual element enhancement, in particular carbon, nitrogen, and oxygen, are needed to further assess whether departures from a strictly solar abundance provide better agreement.

5.2.3 *Helium abundance*

The abundance of helium in the standard models presented thus far is set by assuming the helium mass fraction scales linearly with bulk metallicity from the primordial value $Y_p = 0.2488$ (Peimbert, Luridiana & Peimbert 2007). However, variations in the assumed helium abundance can have a significant impact on stellar models through changes in the mean molecular weight. Reducing the helium abundance effectively leads to a lower $T_{\rm eff}$ and a smaller radius due to reductions in the *p*–*p* chain energy generation rate.

Dartmouth models were generated with $Y = 0.24$, 0.25, 0.26, and 0.278, where the latter value is the solar-calibrated value for a model with solar metallicity. Only by reducing the initial helium abundance of the models below $Y = 0.25$ is it possible to find a model that reproduces the observed properties of HD 189733. It is worrisome that the required helium abundances are below the primordial value, leading us to doubt that helium abundances variations are a plausible explanation.

5.2.4 *Solar mixture*

Along the same lines as reducing the proportion of α-elements and the overall helium abundance, it is possible that the solar heavy element mixture is incorrect in the standard models adopted here. Standard Dartmouth models adopt the abundances from Grevesse & Sauval (1998), despite trends in the literature towards a lower heavy element composition (e.g. Asplund et al. 2009; Caffau et al. 2011). As a test, we computed a set of Dartmouth models adopting the Asplund et al. (2009) solar composition after first re-calibrating the models to the Sun.

We find that it is possible to reproduce the properties of HD 189733 with a 0.80 $M_\odot$ model at an age of 7 Gyr using the Asplund et al. (2009) abundances. It is encouraging that agreement can be found, but caution must be exercised as there are significant unresolved issues between helioseismic data and standard solar models that adopt the Asplund et al. abundances (see e.g. Basu & Antia 2008, 2013). Since solar models calculated with the Asplund et al. abundances do not provide an adequate representation of the solar interior, any agreement found with other stars must be regarded with skepticism.

5.3 Convection

One final aspect of stellar modelling that we wish to address is the efficiency of thermal convection. This is relevant considering recent results from asteroseismic studies, suggesting that convective properties are dependent on intrinsic stellar properties such as mass and composition (Bonaca et al. 2012) and the on-going issue regarding inflated radii of low-mass stars in detached eclipsing binaries (e.g. Torres et al. 2010).

5.3.1 *Reduced* $\alpha_{\rm MLT}$

A simple test is to compute models with various convective mixing-length parameters. Doing so with the Dartmouth models, we find that a mixing-length parameter of $\alpha_{\rm MLT} = 1.4$ is required to bring an 0.81 $M_\odot$ model into agreement with the observations. By comparison, the relationship between stellar properties and convective mixing-length parameter suggested by Bonaca et al. (2012) predicts a mixing length of $\alpha_{\rm MLT} = 1.44$, when re-scaled to the solar-calibrated mixing length in the Dartmouth models. The close agreement may imply that the disagreement between models and the observations is the results of natural variations in convective efficiency. However, we must note that HD 189733, with an empirically determined $T_{\rm eff} = 4875 \pm 43$K is outside of the calibration range of the Bonaca et al. (2012) relation.

5.3.2 *Making constrained models*

Using the directly measured stellar properties, we are able to empirically test how $\alpha_{\rm MLT}$ will change to find agreement with stellar evolutionary models. Although models for HD 209458 do not have difficulty reproducing its observables – likely due to its closer similarity to the Sun – we apply this test on both stars studied here. We use the observed radius, temperature, mass, and associated errors to generate YREC models in a Monte Carlo analysis. In this mode, models are constructed to satisfy the observed mass, radius, temperature, and metallicity constraint. The mixing-length parameter is varied and age (and initial helium abundance) is a free parameter. For each run, mass, radius, effective temperature, and metallicity are varied assuming that their errors have a Gaussian distribution. This requires the code to run in an iterative mode. In all cases only models with ages <13.8 Gyr are chosen. We use standard physics inputs for the models. We use the OPAL equation of state (Rogers & Nayfonov 2002). We use high-temperature opacities from OPAL (Iglesias & Rogers 1996) and supplemented them with low-temperature opacities from Ferguson et al. (2005). We use nuclear reaction rates of Adelberger et al. (1998) except for the $^{14}N(p,\gamma)^{15}O$ reaction, where we use the reaction rate of Formicola et al. (2004). Gravitational settling and diffusion of helium and heavy elements are incorporated using the coefficients of Thoul, Bahcall & Loeb (1994).

Since many of the (mass, radius, $T_{\rm eff}$, Z) combinations for a given mixing-length parameter end up requiring an initial helium abundance less than that produced by the big bang, the results of the Monte Carlo are analysed in two ways. The first way, 'unconstrained', accepts all results. The other way, 'constrained', only allowed results for which the initial helium abundance was greater than the primordial value $Y_p = 0.2488$ (Peimbert et al. 2007). The results of the analysis are shown in Table 4 and in Fig. 4, where the 'constrained' solution for HD 189733 yields $\alpha_{\rm MLT}$=1.34 ± 0.18, a significantly lower $\alpha_{\rm MLT}$ compared to a solar-mass star. This result illustrates that with standard physics, a change in the mixing-length parameter is enough to obtain physical models of the two stars, HD 189733 and HD 209458.

5.3.3 *Magneto-convection*

As an alternative explanation for the reduced convective mixing length, we computed magnetic stellar evolution models using the Dartmouth code DMESTAR (Feiden & Chaboyer 2012, 2013). Two approaches to modelling the influence of the magnetic field were adopted: one that mimics a rotational dynamo by stabilizing convective flows and another whereby convective efficiency is reduced so as to mimic a turbulent dynamo. The magnetic models (of both varieties) require surface magnetic field strengths of approximately 1.5 kG to reproduce the observations. Feiden & Chaboyer (2013)

Table 4. YREC model outputs.

	HD 189733		HD 209458	
Property	Unconstrained	Constrained[a]	Unconstrained	Constrained[a]
$\alpha_{\rm MLT}$	1.65 ± 0.38	1.34 ± 0.18	2.01 ± 0.43	2.01 ± 0.43
Age (Gyr)	5.2 ± 3.5	4.3 ± 2.8	6.5 ± 2.7	6.5 ± 2.7
Initial helium (Y_0)	0.228 ± 0.031	0.266 ± 0.016	0.3240 ± 0.0377	0.3241 ± 0.037
Helium (Y)	0.216 ± 0.032	0.252 ± 0.016	0.2808 ± 0.0388	0.2809 ± 0.0387

[a]With initial helium $Y_0 > 0.2488$.
Note. See Section 5.3.2 for additional details.

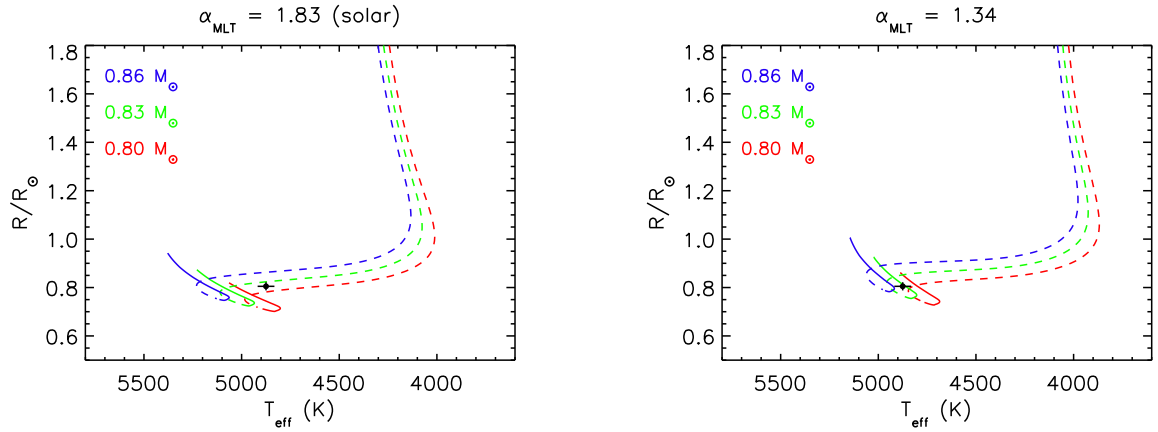

Figure 4. Radius–temperature plot showing the position of HD 189733 with 1σ errors (black point). Each panel also shows evolutionary tracks for the mass indicated in legend, corresponding to the mass of HD 189733 (green), and a range above (blue) and below (red) this value by $\sim 1\sigma$ of the MC analysis. Dashed and solid lines denote pre-MS and MS evolutionary stages, respectively. The left-hand panel shows models using the solar-calibrated $\alpha_{\rm MLT}$, and the right-hand panel shows $\alpha_{\rm MLT}$ parameter found in this work. Note that only models with a reduced $\alpha_{\rm MLT}$ reproduce the observed stellar properties for HD 189733 as a MS star. For details, see Sections 5.3.1 and 5.3.2.

showed that, to a reasonable extent, the interior magnetic field is of less consequence than the surface magnetic field in stars with a radiative core. Thus, the requirement of a 1.5 kG magnetic field is fairly robust, unless super-MG magnetic fields are invoked in the interior. While HD 189733 is fairly active in comparison to the Sun, the measured magnetic field is constrained to be in the range of 40–100 G (Moutou et al. 2007; Pillitteri et al. 2014), considerably lower than required by the models.

5.3.4 Starspots

Finally, HD 189733 is known to show light-curve modulations consistent with the presence of spots on the stellar surface. On short time-scales, spots reduce the flux leaving the stellar surface without influencing the star's radius (e.g. Spruit & Weiss 1986). This would lower the observed luminosity and $T_{\rm eff}$, producing disagreement between models and observations. If we assume that stellar evolution models reproduce the correct radius, but overestimate the $T_{\rm eff}$, then one can estimate the potential spot coverage required to produce the observed luminosity difference.

At the observed radius, standard evolutionary models predict HD 189733 to have a mass consistent with observations of approximately 0.85 $M_{\odot}$, but a luminosity 35 per cent higher than observed. Following Chabrier, Gallardo & Baraffe (2007), this luminosity difference implies spot coverages of between 51–73 per cent if the spots are 25–15 per cent cooler than the surrounding photosphere, respectively. At this level, spots should be detectable either using Dopper Imaging or by modelling spectral features (e.g. O'Neal, Neff & Saar 1998). In fact, this level of spottiness is not consistent with observations of molecular features for even the most active stars (O'Neal et al. 1998). Alternatively, a significant coverage of spots would produce anomalous photometric colours compared to predictions from non-spotted stellar models. However, a 0.85 $M_{\odot}$ stellar model from the Dartmouth series predicts the correct photometric magnitudes and colours. Introducing deviations due to spots produces worse photometric agreement, and is thus unlikely the cause of the offset.

6 SUMMARY

We present direct measurements to the physical properties of two Hall of Fame transiting exoplanet host stars, HD 189733 and HD 209458. We use the CHARA Array to measure the stellar angular diameters. By combining these measurements with distance and bolometric flux, we determine the linear radius, effective temperature, and absolute luminosity for each star (Table 3). Combined with the empirically determined dynamical masses (Snellen et al. 2010; de Kok et al. 2013), and the planet-to-star radius ratio from *Spitzer* data (Agol et al. 2010; Beaulieu et al. 2010), we are able to calculate full system properties for both star and planet independent of models.

We find that the observations of HD 209458 agree with evolutionary model predictions. However, the properties of HD 189733 show discrepancies with models not unlike previously seen with

fundamental measurements of low-mass stars (Boyajian et al. 2012). We consider several scenarios in the attempt to reconcile the differences in either the assumed stellar properties or standard input physics within the models. We conclude that the models will match the data only by adjusting the solar-calibrated mixing-length parameter to a lower value (Section 5.3.1). This work highlights the importance in calibrating $\alpha_{\rm MLT}$ for stars with masses less than the Sun. As such, if models remain unchanged, the trend of models predicting temperatures too high and radii too small will remain. This has significant impact on the field of exoplanet detection and characterization, particularly in the case for low-mass stars too small/faint to be resolved with LBOI (Mann et al. 2013).

The analysis and discussions within this work primarily focus on the discrepancy between our observations and evolutionary model predictions. As such, we do not address in detail comparisons with stellar properties derived with high-resolution spectroscopy, which are heavily model dependent and have sparse empirical verification. However, it is worthy to note that the temperature estimates listed in the PASTEL Catalogue of stellar parameters (Soubiran et al. 2010) for HD 189733 range from 4952 to 5111 K, our temperature being 77 K cooler than the lowest entry. The temperature we measure for HD 209458 falls in the middle of the range in the PASTEL Catalogue (5987–6142 K). We can only speculate the reason for this large discrepancy in the temperature for HD 189733 is due to an extra source of opacity, such as TiO, which begins to appear at this temperature, that is not being correctly accounted for in the models. Another possible reason for the discrepancy is that if the spectroscopic modelling identifies an incorrect $\log g$, this will bias the resulting $T_{\rm eff}$ and metallicity estimates (Buzzoni et al. 2001). Likewise, the semi-empirical approach to determine $T_{\rm eff}$ using the infrared flux method (IRFM; Blackwell, Shallis & Selby 1979) has been refined over the years to incorporate many details with goals to establish an effective temperature scale to better than 1 per cent. While the IRFM is a semi-empirical approach, systematics up to 100 K between IRFM scales (e.g. González Hernández & Bonifacio 2009; Casagrande et al. 2010, and references therein) exist, where the differences may be associated with lack of empirical measurements (i.e. interferometry) to calibrate zero-points (Boyajian et al. 2013). Particularly for stars with $T_{\rm eff} < 5100$ K, IRFM temperatures are systematically hotter by a few per cent (Boyajian et al. 2013, their fig. 2 0). This statement holds true for HD 189733, where the IRFM temperature of 5022 K from Casagrande et al. (2011) is 150 K (3 per cent) hotter than the interferometric $T_{\rm eff}$ derived in this work. The fact that spectroscopic and IRFM estimates of HD 189733's $T_{\rm eff}$ are considerably higher than the interferometric value is further evidence that indirect estimates of cool star properties need to be used with caution until they are able to be calibrated with empirical data sets.

A further implication of the corrections to stellar parameters is the calculated extent of the Habitable Zone (HZ; Kopparapu 2013; Kopparapu et al. 2014). Kane (2014) quantified the importance of stellar parameter determinations in defining the HZ boundaries for a particular system. Although the known planets in the systems studied in this paper cannot be consider HZ planets, the divergence of the measured stellar parameters from stellar models will have serious consequences for correct determinations of the fraction of stars with Earth-sized planets in the HZ ($\eta_\oplus$). This is particular true for late-type stars since (i) the short-period bias of the transit and radial velocity methods is preferentially revealing $\eta_\oplus$ for this stellar population, and (ii) calculated late-type stellar properties tend to have the largest divergence from models. It is therefore of critical importance to consider these results when describing HZ regions for current and upcoming targets, such as those of the *Transiting Exoplanet Survey Satellite* (Ricker 2014).

ACKNOWLEDGEMENTS

TSB acknowledges support provided through NASA grants ADAP12-0172 and 14-XRP14_2-0147. DH acknowledges support by NASA Grant NNX14AB92G issued through the Kepler Participating Scientist Program. SB acknowledges partial support of NSF grant AST-1105930. Judit Sturmann keeps some tight beams in place – hats off to you girl! The CHARA Array is funded by the National Science Foundation through NSF grants AST-0606958 and AST-0908253 and by Georgia State University through the College of Arts and Sciences, as well as the W. M. Keck Foundation. This research made use of the SIMBAD and VIZIER Astronomical Databases, operated at CDS, Strasbourg, France (http://cdsweb.u-strasbg.fr/), and of NASA's Astrophysics Data System, of the Jean-Marie Mariotti Center `SearchCal` service (http://www.jmmc.fr/searchcal), co-developed by FIZEAU and LAOG/IPAG.

REFERENCES

Absil O. et al., 2008, A&A, 487, 1041
Adelberger E. G. et al., 1998, Rev. Mod. Phys., 70, 1265
Agol E., Cowan N. B., Knutson H. A., Deming D., Steffen J. H., Henry G. W., Charbonneau D., 2010, ApJ, 721, 1861
Aldering G. et al., 2002, in Tyson J. A., Wolff S., eds, Proc. SPIE. Conf. Ser. Vol. 4836, Survey and Other Telescope Technologies and Discoveries. SPIE, Bellingham, p. 61
Aldering G. et al., 2006, ApJ, 650, 510
Árnadóttir A. S., Feltzing S., Lundström I., 2010, A&A, 521, A40
Asplund M., Grevesse N., Sauval A. J., Scott P., 2009, ARA&A, 47, 481
Aumer M., Binney J. J., 2009, MNRAS, 397, 1286
Bacon R. et al., 2001, MNRAS, 326, 23
Bailer-Jones C. A. L., 2011, MNRAS, 411, 435
Baines E. K., van Belle G. T., ten Brummelaar T. A., McAlister H. A., Swain M., Turner N. H., Sturmann L., Sturmann J., 2007, ApJ, 661, L195
Baines E. K., McAlister H. A., ten Brummelaar T. A., Turner N. H., Sturmann J., Sturmann L., Goldfinger P. J., Ridgway S. T., 2008, ApJ, 680, 728
Baines E. K. et al., 2012, ApJ, 761, 57
Bakos G. Á., Pál A., Latham D. W., Noyes R. W., Stefanik R. P., 2006, ApJ, 641, L57
Basu S., Antia H. M., 2008, Phys. Rep., 457, 217
Basu S., Antia H. M., 2013, J. Phys. Conf. Ser., 440, 012017
Beaulieu J. P. et al., 2010, MNRAS, 409, 963
Bessell M., Murphy S., 2012, PASP, 124, 140
Blackwell D. E., Shallis M. J., Selby M. J., 1979, MNRAS, 188, 847
Bohlin R. C., Gordon K. D., Tremblay P. E., 2014, PASP, 126, 711
Bonaca A. et al., 2012, ApJ, 755, L12
Bonneau D. et al., 2006, A&A, 456, 789
Bonneau D., Delfosse X., Mourard D., Lafrasse S., Mella G., Cetre S., Clausse J. M., Zins G., 2011, A&A, 535, A53
Bouchy F. et al., 2005, A&A, 444, L15
Boyajian T. S. et al., 2008, ApJ, 683, 424
Boyajian T. S. et al., 2012, ApJ, 757, 112
Boyajian T. S. et al., 2013, ApJ, 771, 40
Boyajian T. S., van Belle G., von Braun K., 2014, AJ, 147, 47
Buton C. et al., 2013, A&A, 549, A8
Buzzoni A., Chavez M., Malagnini M. L., Morossi C., 2001, PASP, 113, 1365
Caffau E., Ludwig H. G., Steffen M., Freytag B., Bonifacio P., 2011, Sol. Phys., 268, 255
Carter J. A. et al., 2011, Science, 331, 562
Casagrande L., Ramírez I., Meléndez J., Bessell M., Asplund M., 2010, A&A, 512, A54

Casagrande L., Schönrich R., Asplund M., Cassisi S., Ramírez I., Meléndez J., Bensby T., Feltzing S., 2011, A&A, 530, A138
Chabrier G., Gallardo J., Baraffe I., 2007, A&A, 472, L17
Charbonneau D., Brown T. M., Latham D. W., Mayor M., 2000, ApJ, 529, L45
Claret A., Bloemen S., 2011, A&A, 529, A75
Cody A. M., Sasselov D. D., 2002, ApJ, 569, 451
Cushing M. C., Vacca W. D., Rayner J. T., 2004, PASP, 116, 362
Cutri R. M. et al., 2003, The 2MASS All Sky Catalog of Point Sources. IPAC, Pasadena, CA
de Kok R. J., Brogi M., Snellen I. A. G., Birkby J., Albrecht S., de Mooij E. J. W., 2013, A&A, 554, A82
de Kok R. J., Birkby J., Brogi M., Schwarz H., Albrecht S., de Mooij E. J. W., Snellen I. A. G., 2014, A&A, 561, A150
Demarque P., Woo J. H., Kim Y. C., Yi S. K., 2004, ApJS, 155, 667
Dotter A., Chaboyer B., Jevremović D., Kostov V., Baron E., Ferguson J. W., 2008, ApJS, 178, 89
Doyle L. R. et al., 2011, Science, 333, 1602
Droege T. F., Richmond M. W., Sallman M. P., Creager R. P., 2006, PASP, 118, 1666
Feiden G. A., Chaboyer B., 2012, ApJ, 761, 30
Feiden G. A., Chaboyer B., 2013, ApJ, 779, 183
Ferguson J. W., Alexander D. R., Allard F., Barman T., Bodnarik J. G., Hauschildt P. H., Heffner-Wong A., Tamanai A., 2005, ApJ, 623, 585
Formicola A. et al., 2004, Phys. Lett. B, 591, 61
Gaidos E. et al., 2014, MNRAS, 443, 2561
González Hernández J. I., Bonifacio P., 2009, A&A, 497, 497
Gray R. O., Napier M. G., Winkler L. I., 2001, AJ, 121, 2148
Gray R. O., Corbally C. J., Garrison R. F., McFadden M. T., Robinson P. E., 2003, AJ, 126, 2048
Grevesse N., Sauval A. J., 1998, Space Sci. Rev., 85, 161
Guinan E. F., 2013, J. Am. Assoc. Var. Star Obs., 41, 153
Hanbury Brown R. H., Davis J., Lake R. J. W., Thompson R. J., 1974, MNRAS, 167, 475
Hauck B., Mermilliod M., 1998, A&AS, 129, 431
Henry G. W., Marcy G. W., Butler R. P., Vogt S. S., 2000, ApJ, 529, L41
Høg E. et al., 2000, A&A, 355, L27
Huber D. et al., 2012, ApJ, 760, 32
Huber D. et al., 2013, ApJ, 767, 127
Iglesias C. A., Rogers F. J., 1996, ApJ, 464, 943
Ireland M. J. et al., 2008, in Schöller M., Danchi W. C., Delplancke F., eds, Proc. SPIE Conf. Ser. Vol. 7013, Optical and Infrared Interferometry. SPIE, Bellingham, p. 63
Kane S. R., 2014, ApJ, 782, 111
Kharchenko N. V., 2001, Kinematika Fiz. Nebesnykh Tel, 17, 409
Kharchenko N. V., Scholz R. D., Piskunov A. E., Röser S., Schilbach E., 2007, Astron. Nachr., 328, 889
Koen C., Kilkenny D., van Wyk F., Marang F., 2010, MNRAS, 403, 1949
Kopparapu R. K., 2013, ApJ, 767, L8
Kopparapu R. K., Ramirez R. M., SchottelKotte J., Kasting J. F., Domagal-Goldman S., Eymet V., 2014, ApJ, 787, L29
Kotoneva E., Flynn C., Chiappini C., Matteucci F., 2002, MNRAS, 336, 879
Lantz B. et al., 2004, in Mazuray L., Rogers P. J., Wartmann R., eds, Proc. SPIE Conf. Ser. Vol. 5249, Optical Design and Engineering. SPIE, Bellingham, p. 146
Maestro V. et al., 2013, MNRAS, 434, 1321
Malo L., Doyon R., Feiden G. A., Albert L., Lafrenière D., Artigau É., Gagné J., Riedel A., 2014, ApJ, 792, 37
Mann A. W., von Braun K., 2014, preprint (arXiv:1412.1474)
Mann A. W., Gaidos E., Ansdell M., 2013, ApJ, 779, 188
Mishenina T. V., Soubiran C., Kovtyukh V. V., Katsova M. M., Livshits M. A., 2012, A&A, 547, A106
Mishenina T. V., Pignatari M., Korotin S. A., Soubiran C., Charbonnel C., Thielemann F. K., Gorbaneva T. I., Basak N. Y., 2013, A&A, 552, A128
Moutou C. et al., 2007, A&A, 473, 651
Muirhead P. S. et al., 2014, ApJS, 213, 5
O'Neal D., Neff J. E., Saar S. H., 1998, ApJ, 507, 919
Oke J. B., 1990, AJ, 99, 1621
Olsen E. H., 1983, A&AS, 54, 55
Olsen E. H., 1993, A&AS, 102, 89
Olsen E. H., 1994, A&AS, 106, 257
Peimbert M., Luridiana V., Peimbert A., 2007, ApJ, 666, 636
Perryman M. A. C. et al. 1997, A&A, 323, L49
Pillitteri I., Wolk S. J., Cohen O., Kashyap V., Knutson H., Lisse C. M., Henry G. W., 2010, ApJ, 722, 1216
Pillitteri I., Wolk S. J., Lopez-Santiago J., Günther H. M., Sciortino S., Cohen O., Kashyap V., Drake J. J., 2014, ApJ, 785, 145
Ramírez I., Meléndez J., 2005, ApJ, 626, 465
Rayner J. T., Toomey D. W., Onaka P. M., Denault A. J., Stahlberger W. E., Vacca W. D., Cushing M. C., Wang S., 2003, PASP, 115, 362
Ricker G. R., 2014, J. Am. Assoc. Var. Star Obs., 42, 234
Rodler F., Kürster M., Barnes J. R., 2013, MNRAS, 432, 1980
Rogers F. J., Nayfonov A., 2002, ApJ, 576, 1064
Seager S., 2011, Exoplanets. Univ. Arizona Press, Tucson, AZ
Seager S., Mallén-Ornelas G., 2003, ApJ, 585, 1038
Snellen I. A. G., de Kok R. J., de Mooij E. J. W., Albrecht S., 2010, Science, 465, 1049
Soubiran C., Le Campion J. F., Cayrel de Strobel G., Caillo A., 2010, A&A, 515, A111
Southworth J., 2009, MNRAS, 394, 272
Southworth J., 2010, MNRAS, 408, 1689
Southworth J., 2011, MNRAS, 417, 2166
Sozzetti A., Torres G., Charbonneau D., Latham D. W., Holman M. J., Winn J. N., Laird J. B., O'Donovan F. T., 2007, ApJ, 664, 1190
Spada F., Demarque P., Kim Y. C., Sills A., 2013, ApJ, 776, 87
Spruit H. C., Weiss A., 1986, A&A, 166, 167
Thoul A. A., Bahcall J. N., Loeb A., 1994, ApJ, 421, 828
Torres G., 2007, ApJ, 671, L65
Torres G., Winn J. N., Holman M. J., 2008, ApJ, 677, 1324
Torres G., Andersen J., Giménez A., 2010, A&AR, 18, 67
Vacca W. D., Cushing M. C., Rayner J. T., 2003, PASP, 115, 389
van Belle G. T., van Belle G., 2005, PASP, 117, 1263
van Belle G. T., von Braun K., 2009, ApJ, 694, 1085
van Leeuwen F., 2007, A&A, 474, 653
von Braun K. et al., 2011, ApJ, 740, 49
von Braun K. et al., 2012, ApJ, 753, 171
von Braun K. et al., 2014, MNRAS, 438, 2413
Welsh W. F. et al., 2012, Science, 481, 475
White T. R. et al., 2013, MNRAS, 433, 1262
Winn J. N., 2010, preprint (arXiv:1001.2010)
Yi S., Demarque P., Kim Y. C., Lee Y. W., Ree C. H., Lejeune T., Barnes S., 2001, ApJS, 136, 417
Yi S. K., Kim Y. C., Demarque P., 2003, ApJS, 144, 259

[1]*Yale University, New Haven, CT 06520, USA*
[2]*Max-Planck-Institute for Astronomy (MPIA), Königstuhl 17, D-69117 Heidelberg, Germany*
[3]*Mirasol Institute, D-81679 Munich, Germany*
[4]*Lowell Observatory, Flagstaff 86001, USA*
[5]*Department of Physics & Astronomy, Uppsala University, Box 516, SE-751 20 Uppsala, Sweden*
[6]*NASA Ames Research Center, Moffett Field, CA 94035, USA*
[7]*SETI Institute, 189 Bernardo Avenue, Mountain View, CA 94043, USA*
[8]*The CHARA Array, Mount Wilson Observatory, Mount Wilson, CA 91023, USA*
[9]*Department of Astronomy, The University of Texas at Austin, Austin, TX 78712, USA*
[10]*Institut für Astrophysik, Georg-August-Universität Göttingen, Friedrich-Hund-Platz 1, D-37077 Göttingen, Germany*
[11]*Sydney Institute for Astronomy, School of Physics, University of Sydney, NSW 2006, Australia*

[12]*Leibniz-Institut für Astrophysik Potsdam (AIP), An der Sternwarte 16, D-14482 Potsdam, Germany*
[13]*Harvard–Smithsonian Center for Astrophysics, 60 Garden Street, Cambridge, MA 03128, USA*
[14]*Research School of Astronomy & Astrophysics, Australian National University, Canberra, ACT 2611, Australia*
[15]*Department of Physics and Astronomy, San Francisco State University, 1600 Holloway Ave, San Francisco, CA 94132, USA*
[16]*Center for High Angular Resolution Astronomy and Department of Physics and Astronomy, Georgia State University, Atlanta, GA 30303, USA*
[17]*NASA Exoplanet Science Institute, California Institute of Technology, MC 100-22, Pasadena, CA 91125, USA*
[18]*NOAO, Tucson, AZ 85719, USA*

This paper has been typeset from a TEX/LATEX file prepared by the author.